

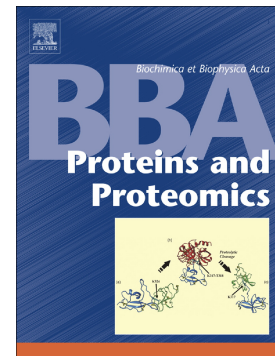
This is the Post-print version of the following article: *Pedro Jimenez-Sandoval, Jose Luis Vique-Sanchez, Marisol López Hidalgo, Gilberto Velazquez-Juarez, Corina Diaz-Quezada, Luis Fernando Arroyo-Navarro, Gabriela Montero Moran, Juliana Fattori, A. Jessica Diaz-Salazar, Enrique Rudiño-Pinera, Rogerio Sotelo-Mundo, Ana Carolina Migliorini Figueira, Samuel Lara-Gonzalez, Claudia G. Benítez-Cardoza, Luis G. Brieba, A competent catalytic active site is necessary for substrate induced dimer assembly in triosephosphate isomerase, Biochimica et Biophysica Acta (BBA) - Proteins and Proteomics, Volume 1865, Issue 11, Part A, 2017, Pages 1423-1432, which has been published in final form at: <https://doi.org/10.1016/j.bbapap.2017.07.014>*

© 2017. This manuscript version is made available under the Creative Commons Attribution-NonCommercial-NoDerivatives 4.0 International (CC BY-NC-ND 4.0) license <http://creativecommons.org/licenses/by-nc-nd/4.0/>

Accepted Manuscript

A competent catalytic active site is necessary for substrate induced dimer assembly in triosephosphate isomerase

Pedro Jimenez-Sandoval, Jose Luis Vique-Sanchez, Marisol López Hidalgo, Gilberto Velazquez-Juarez, Corina Diaz-Quezada, Luis Fernando Arroyo-Navarro, Gabriela Montero Moran, Juliana Fattori, A. Jessica Diaz-Salazar, Enrique Rudiño-Pinera, Rogerio Sotelo-Mundo, Ana Carolina Migliorini Figueira, Samuel Lara-Gonzalez, Claudia G. Benítez-Cardoza, Luis G. Briebe



PII: S1570-9639(17)30169-3
DOI: doi: [10.1016/j.bbapap.2017.07.014](https://doi.org/10.1016/j.bbapap.2017.07.014)
Reference: BBAPAP 39979

To appear in:

Received date: 9 June 2017
Revised date: 7 July 2017
Accepted date: 24 July 2017

Please cite this article as: Pedro Jimenez-Sandoval, Jose Luis Vique-Sanchez, Marisol López Hidalgo, Gilberto Velazquez-Juarez, Corina Diaz-Quezada, Luis Fernando Arroyo-Navarro, Gabriela Montero Moran, Juliana Fattori, A. Jessica Diaz-Salazar, Enrique Rudiño-Pinera, Rogerio Sotelo-Mundo, Ana Carolina Migliorini Figueira, Samuel Lara-Gonzalez, Claudia G. Benítez-Cardoza, Luis G. Briebe, A competent catalytic active site is necessary for substrate induced dimer assembly in triosephosphate isomerase, (2017), doi: [10.1016/j.bbapap.2017.07.014](https://doi.org/10.1016/j.bbapap.2017.07.014)

This is a PDF file of an unedited manuscript that has been accepted for publication. As a service to our customers we are providing this early version of the manuscript. The manuscript will undergo copyediting, typesetting, and review of the resulting proof before it is published in its final form. Please note that during the production process errors may be discovered which could affect the content, and all legal disclaimers that apply to the journal pertain.

A competent catalytic active site is necessary for substrate induced dimer assembly in triosephosphate isomerase

Pedro Jimenez-Sandoval ^a, Jose Luis Vique-Sanchez ^b, Marisol López Hidalgo^b, Gilberto Velazquez-Juarez ^c, Corina Diaz-Quezada ^a, Luis Fernando Arroyo-Navarro ^a, Gabriela Montero Moran ^a, Juliana Fattori ^d, A. Jessica Diaz-Salazar ^e, Enrique Rudiño-Pinera ^f, Rogerio Sotelo-Mundo^g, Ana Carolina Migliorini Figueira ^d, Samuel Lara-Gonzalez ^h Claudia G. Benítez-Cardoza ^b, Luis G. Briebe ^{a*}

^a Laboratorio Nacional de Genómica para la Biodiversidad, Centro de Investigación y de Estudios Avanzados del IPN, Apartado Postal 629, CP 36821, Irapuato, Guanajuato, México.

^b Laboratorio de Investigación Bioquímica, Programa Institucional en Biomedicina Molecular ENMyH-IPN, Guillermo Massieu Helguera No. 239, La Escalera Ticoman, 07320, D.F, México.

^c Universidad de Guadalajara, Centro Universitario de Ciencias Exactas e Ingenierías. Departamento de Química. Blvd. Marcelino García Barragán, Ciudad Universitaria, 44430 Guadalajara, México.

^d Laboratório Nacional de Biociências - LNBio/ Centro Nacional de Pesquisa em Energia e Materiais - CNPEM Rua Giuseppe Máximo Scolfaro, n.º 10.000 - Guara |Caixa Postal 6192 | CEP 13.083-970 | Campinas - SP| Brasil

^e Laboratorio de Biofísica, Departamento de Fisicoquímica, Facultad de Química, Universidad Nacional Autónoma de México. México D.F. CP 04510, México.

^f Instituto de Biotecnología, UNAM. Av. Universidad 2001, Chamilpa, 62210 Cuernavaca, Morelos, México.

^g Laboratorio de Estructura Biomolecular. Centro de Investigación en Alimentación y Desarrollo, A.C. (CIAD). Carretera a Ejido La Victoria Km 0.6, Apartado Postal 1735, Hermosillo, Sonora, 83304 México.

^h IPICYT, División de Biología Molecular, Camino a la Presa San José 2055, CP 78216. San Luis Potosí, San Luis Potosí, México.

*To whom correspondence should be addressed:

luis.briebe@cinvestav.mx

Running title:

Dimer assembly in triosephosphate isomerase

ABSTRACT

The protozoan parasite *Trichomonas vaginalis* contains two nearly identical triosephosphate isomerases (TvTIMs) that dissociate into stable monomers and dimerize upon substrate binding. Herein, we compare the role of the “ball and socket” and loop 3 interactions in substrate assisted dimer assembly in both TvTIMs. We found that point mutants at the “ball” are only 39 and 29-fold less catalytically active than their corresponding wild-type counterparts, whereas Δ loop 3 deletions are 1502 and 9400-fold less active. Point and deletion mutants dissociate into stable monomers. However, point mutants assemble as catalytic competent dimers upon binding of the transition state substrate analog PGH, whereas loop 3 deletions remain monomeric. A comparison between crystal structures of point and loop 3 deletion monomeric mutants illustrates that the catalytic residues in point mutants and wild-type TvTIMs are maintained in the same orientation, whereas the catalytic residues in deletion mutants show an increase in thermal mobility and present structural disorder that may hamper their catalytic role. The high enzymatic activity present in monomeric point mutants correlates with the formation of dimeric TvTIMs upon substrate binding. In contrast, the low activity and lack of dimer assembly in deletion mutants suggests a role of loop 3 in promoting the formation of the active site as well as dimer assembly. Our results suggest that in TvTIMs the active site is assembled during dimerization and that the integrity of loop 3 and ball and socket residues is crucial to stabilize the dimer.

INTRODUCTION

Proteins assemble as oligomers to promote cooperativity, increase thermal stability or to prevent protein degradation [1, 2]. In most species, triosephosphate isomerase (TIM) is a homodimer, with the exception of archaea in which this enzyme assembles into a tetramer [3-6]. Because of the reduced catalytic activity of monomeric TIMs and the high stability of their dimers, this enzyme is referred as an obligated dimer [7-10]. TIMs assemble as $(\beta-\alpha)_8$ barrels with limited amino acid sequence identity between its members [7, 11-13]. Although this limited sequence identity, crystal structures of more than 40 dimeric TIMs are superimposable, indicating the high conservation of the structural elements present in this enzyme.

TIMs form stable dimers and their association constants rank between 10^{11} M^{-1} to 10^{14} M^{-1} [14, 15]. TIM dimers are assembled by an extended hydrophobic surface in which one monomer packs against its neighbor monomer using an extended structural element of approximately 16 amino acids dubbed loop 3 [11, 12, 16]. Several engineered monomeric TIMs using loop 3 deletions produced monomeric enzymes that decrease their catalytic efficiency between 500 to 25,000 times with respect to their wild-type enzymes [17-20]. This considerable decrease in catalytic efficiency is measurable because of the large enzymatic activity present in TIMs. It is suggested that the decrease in catalytic activity of those monomeric mutants is because they exhibit an increased flexibility in their catalytic Lys and His residues [17-19]. In contrast, several point mutants that disrupt the interface have a moderate effect on activity and are not totally monomeric [7, 9].

Trichomonas vaginalis is a protozoan parasite that suffered a duplication event of its *tpi* gene and one or both TvTIMs localize to the parasite's surface and contribute to cell adhesion [21]. TvTIMs only differ in four amino acids and from these four amino acids, residue 45 (Ile or Val) is located at the dimer interface forming a "ball and socket" interplay with a hydrophobic cavity of the adjacent monomer [16, 22]. Despite these proteins only differ in 4 of their 252 amino acids, the dimer of TvTIM1 is 20 kJ mol^{-1} more stable than the dimer of TvTIM2. Mutations of Ile 45 or Val 45 to Ala yield monomeric TvTIMs even at high protein concentrations [23]. In contrast to all TIMs studied to date, the energy necessary to unfold a TvTIM monomer is greater than the energy necessary to dissociate the dimer [16].

TvTIMs monomers are stable and assemble as dimers upon the binding of a transition state substrate analog [23]. Thermodynamic studies indicate that protein stability is not the only reason that accounts for TIM dimerization suggesting that dimerization and enzymatic activity must be intimately correlated [24]. In order to gain insights in the dimeric nature of TIMs, we decided to revisit a set of deletions in loop 3 of TvTIMs that yield monomeric enzymes and compared the structural and biophysical properties of these proteins with respect to monomeric TvTIMs engineered by single point mutations of residue 45 Ile (Val or Ala) at the ball and socket interaction [16, 23].

RESULTS

THE DIMER INTERFACE OF TVTIMS HAS TWO MAIN COMPONENTS: A BALL AND SOCKET INTERACTION AND INTERMOLECULAR LOOP 3 SWAPPING

In TIMs the dimer interface consists of inter-subunit interactions between loop3 and a crevice formed between loop 1 and loop 4 of the neighboring subunit [25, 26]. In TvTIMs, loop 3 is located between residues Ala62 to Pro80 [16]. The “ball and socket” interaction consist of the side chain of residue 45 packed against a hydrophobic pocket formed with amino acids from α helices 2 and 3 [16, 23]. The character of the “ball” at position 45 is an Ile or a Val in TvTIM1 and TvTIM2 respectively. In order to test the relative contributions of residue 45 and loop 3 in dimer stability and catalytic efficiency, we studied two previously reported point alanine mutants of residue 45 in TvTIMs in comparison to their loop3 deletions [16, 23]. Using the crystal structures of TvTIM1 and TvTIM2 we designed a shorter version of loop 3 by deleting six residues between residues Gly71 to Thr78 (**Fig. S1**). Loop3 deletions promote monomerization in other TIMs [17-19] (**Fig. 1A**). The deletion of 6 amino acids contributes to a theoretical decrease of $\sim 700 \text{ \AA}^2$ in the interface surface area of dimeric TvTIMs. In contrast to this large decrease, TvTIM1-Ile45Ala and TvTIM2-Val45Ala point mutants decrease the area of interaction between monomers in ~ 70 and 50 \AA^2 respectively [16].

MUTANTS WITH A BALL AND SOCKET INTERACTIONS DISPLAY MONOMER-DIMER EQUILIBRIUM

Proteins were expressed in a Δtpi bacterial strain, purified to homogeneity and concentrated to 1 mg ml⁻¹. At this protein concentration, wild-type TvTIM1 elutes in a volume that corresponds to a dimer of 46 kDa (black trace). This elution profile contrasts with the elution profiles of point and deletion mutants. TvTIM1-Ile45Ala (red trace), TvTIM2-Val45Ala (magenta trace), TvTIM1- Δ loop3 (blue trace), and TvTIM2- Δ loop3 (orange trace) present elution profiles that correspond to a monomer of approximately 23 kDa and present minimal dimer formation (**Fig. 1B and C**). The elution profiles of TvTIM- Δ loop3 deletions is in agreement with the elution profiles of monomeric TIMs created by altering this loop in *T. cruzi* and *T. brucei* [14, 18, 19]. Thus, in TvTIMs point mutants that eliminate two or one methyl groups and deletion mutants that eliminate six amino acids yield monomeric TvTIMs. As observed in a SDS-PAGE gel, highly purified proteins were used to run these chromatographs (**Fig. 1D**).

POINT MUTANTS BUT NOT DELETION MUTANTS ARE ABLE TO COMPLEMENT Δ TPI *E. COLI* STRAIN

In order to quantify the possible differences in complementation between point and deletion mutants, we transformed plasmids harboring these TvTIM mutants into an *E. coli* BL21 DE3 Δtpi strain [13]. We used glycerol as the sole carbon source as complementation, because this carbon source is more stringent than lactate [27]. Wild-type and point mutants were able to complement an *E. coli* deficient Δtpi strain in agar medium, whereas deletion mutants were not able to complement after 48 h (**Fig. 2A**) or 72 h of incubation (data not shown). Bacteria complemented with wild-type and point mutants growth in liquid medium, whereas bacteria complemented with deletion mutants did not growth in media with glycerol as carbon source (**Fig. 2B**). The *in vivo* complementation assay indicated that monomeric point mutants are sufficiently active to avoid the production of toxic methylglyoxal and complement a Δtpi *E. coli* strain, whereas Δ loop3 deletion mutants are inactive or not sufficiently active to achieve complementation.

POINT MUTANTS PRESENT SIMILAR KINETIC PARAMETERS AS WILD-TYPE TVTIMS, WHEREAS DELETION MUTANTS ARE CATALYTICALLY DEFICIENT

TIMs display catalytic efficiencies in the order of $1 \times 10^5 \text{ mM}^{-1} \text{ min}^{-1}$ and their catalysis is diffusion controlled [22, 28]. The catalytic activities of TvTIM1 and TvTIM2 are similar to other TIMs [22]. As previously reported, mutant TvTIM1-Ile45Ala increases the K_M for G3P by 1.7-fold and present a 17-fold reduction in its k_{cat} [23], whereas TvTIM2-Val45Ala mutant increases the K_M for G3P by 2.14-fold and reduces the k_{cat} 18-fold (**Table 1**). TvTIM- Δ loop3 mutants increase the K_M for G3P by ~ 2 -fold whereas their k_{cat} decreases more than a thousand-fold (**Table 1**). The analysis of the steady-state kinetic parameters for TvTIM point and deletion mutants indicate that alanine point mutants of residue 45 present a 29 and 39-fold decrease in catalytic efficiency, whereas TvTIM deletion mutants exhibit a 1502 and 9400-fold decrease in catalytic efficiency (**Table 1**).

CHEMICAL UNFOLDING OF TVTIMS

To further investigate if the differences in enzymatic activities between point and deletion monomeric mutants can be attributed to changes in protein stability, we assessed their chemical unfolding by monitoring their intrinsic fluorescence at a protein concentration of $30 \mu\text{g ml}^{-1}$, calculating their denaturation profiles in Gdn-HCl and comparing the results with previously reported values for point mutants [16, 23] (**Figure 3A, 3B**). The transition profiles indicate that point and deletion mutants are monomeric and follow a three-state denaturation model: $N \leftrightarrow I \leftrightarrow D$ previously described for monomeric mutants [23]. In this model, N represents the native monomer; I, stands for an intermediate species populated in the unfolding pathway, and D represents the chemically unfolded conformation for each of the enzymes (**Table 2**). The free energy change of the first denaturation transition corresponds to the conformational change from the native state to become the intermediate species. TvTIM2- Δ loop3 shows the lowest value, (12 kJ mol^{-1}), followed by TvTIM1- Δ loop3 (15.3 kJ mol^{-1}), TvTIM1-Val45Ala (16.7 kJ mol^{-1}), and TvTIM1-Ile45Ala (27.1 kJ mol^{-1}). The free energy change associated with the formation of the fully unfolded protein from the intermediate species ($\Delta G_{ID}^{H_2O}$) is very similar in TvTIM2-Val45Ala, TvTIM2- Δ loop3, and TvTIM1- Δ loop3 (on average 28.7 kJ mol^{-1}), whereas TvTIM1-Ile45Ala is slightly more stable (39.2 kJ mol^{-1}). The free energy change corresponding to the complete unfolding of the monomeric constructs ($\Delta G_{ND}^{H_2O}$), was calculated to be between 40 and 66 kJ mol^{-1} . TvTIM2-Val45Ala, TvTIM2- Δ loop3 and TvTIM1- Δ loop3 present a similar stability (40 ± 3.0 to $46.9 \pm 3.2 \text{ kJ mol}^{-1}$) whereas point mutant TvTIM1-Ile45Ala is more stable ($66.3 \pm 4.0 \text{ kJ mol}^{-1}$).

The dye 1-anilino-8-naphthalenesulfonate (ANS) binds to hydrophobic regions and is used to determine folding intermediates or hydrophobic regions on proteins. Point and deletion mutants display different accessibility to ANS upon denaturation by Gdn-HCl (**Figure 3C, 3D**). Wild-type TvTIMs dissociate creating an area of great affinity to ANS at 1M Gdn-HCl than the observed ANS interaction present in monomeric variants.

A SUBSTRATE ANALOG INDUCES DIMER FORMATION MAINLY IN POINT MUTANTS

The high catalytic efficiency of point mutants in residue Ile45 of TvTIM1 is explained by the capacity of substrate to induce dimer assembly [23]. In order to understand if the differences in enzymatic activity could be correlated with differences in substrate binding, we measured the dimer-monomer equilibrium for TvTIMs point and deletion mutants using increasing concentrations of the transition state analog phosphoglycolohydroxamate (PGH) by analytical ultracentrifugation (AUC) (**Figure 4 and Table 3**). AUC analysis indicate that point mutants assemble as dimers in the presence of increasing concentrations of PGH. TvTIM1-Ile45Ala and TvTIM2-Val45Ala are populated as 68% and 73% of dimers at 0.75 mM of PGH. However, loop 3 deletion mutants do not exhibit an increase in their dimer population upon the addition of PGH even at a concentration of 0.75 mM (**Figure 4**).

CRYSTAL STRUCTURES OF POINT AND DELETION MUTANTS SUGGESTAR THAT DELETION MUTANTS ALTER THE ACTIVE SITE

Crystal structure of several engineered monomeric TIMs from *T. brucei* and *T. cruzi* shown that loop 3 deletions increases flexibility in loops 1, 4, and 8, and that this flexibility alters the orientation of catalytic residues thereby decreasing catalysis [18-20]. In order to understand the differences in catalytic activities for point and deletion mutants we solved the crystal structures of TvTIM1- Δ loop3, TvTIM2- Δ loop3, and TvTIM2-Val45Ala and compared them with the previously reported crystal structures of their corresponding wild-types and TvTIM1-Ile45Ala [16, 23] (**Table S1**). All mutants crystallized in space group P2₁2₁2 with one monomer per asymmetric unit that assembled as a biological unit of a dimer (**Figure S2**). An electron density omit map of each mutants allows the visualization of the alanine

point mutations at residue 45 (**Figure S3**). The crystal structures of point mutants TvTIM1-Ile45Ala and TvTIM2-Val45Ala are practically identical to their corresponding wild-types with rmsd values near 0.3 Å between them. Deletion of loop3 eliminates 6 amino acids between Gly71 and Thr78. In contrast to the complete amino acid assignment present in the crystal structures of point mutants, TvTIM1- Δ loop3 mutant lacks electron density for residues Lys68, Pro69, Asn70, and Gly71 of loop3 and residues 99 to 103 that are located in a loop between β 4 and α 4. The electron density maps of TvTIM2- Δ loop3 mutant lack electron density for residues Pro69 and Asn70 and residues 89 to 97 (**Figure S2**). Despite their overall structural similarity, point mutants TvTIM1-Ile45Ala and TvTIM2-Val45Ala present subtle differences with respect to their wild-type counterparts. The main changes are associated with the repacking of residues Phe44, Leu47, Ala62, and Phe85 that contribute to a decrease in the volume of the socket. For instance, the volume of the socket decreases from 46 Å³ in wild-type TvTIM1 to 21 Å³ in the TvTIM1-Ile45Ala. In the case of TvTIM2 the socket has a volume of 31 Å³ and this volume decreases to 18 Å³ in the TvTIM2-Val45Ala mutant. These subtle changes in the socket are correlated with an increase in normalized B-factor values (**Figure 5**). In the case of deletion mutants, the changes in structural mobility are more severe. Increasing B-factors values are observed in α helices 4 and 5. Point mutants present basically the same surface area as their wild-type counterparts. However, the deletion of loop 3 severely decreases the surface area between monomers (**Table S2 and Figure S3**). The deletion of loop 3 originates changes in the position of α helix 4 and repacking of the N-terminal segment of loop 3. The rotation of the α helices and movement of loop 3 alters the orientation of catalytic amino acids (**Figure 6**). The imidazole side chain of His94 rotates into a non-catalytic conformation and the side chain of Lys11 is translated with respect to its position in wild-type TvTIMs (**Figure 6**). The movement of the catalytically conserved amino acids contrast to the active site amino acids of alanine point mutants that do not present changes in the orientation of their catalytic amino acids.

DISCUSSION

Herein we used two different versions of monomeric TvTIM proteins to understand how substrate drives dimerization. The TvTIM dimer interface encompasses more than 1600 Å², so it is puzzling how alanine mutants at position 45 that only decrease the surface area by 70 or 50 Å² turns TvTIMs into monomers. In contrast, deletion of loop 3 decrease the

interface area between subunits by nearly 50% and deletions of this loop are widely used to create monomeric TIMs [14, 17, 20, 29] (**Table S2**). Both point and deletion TvTIM mutants are monomeric proteins even at concentration as high as 1 mg ml⁻¹. However, monomeric TvTIM mutants present contrasting differences in enzymatic activity. In the case of point alanine mutants, their catalytic efficiency decreases by 30 and 40-fold, whereas loop 3 deletion mutants decrease their activity by 1500 and 9400-fold. The decrease in enzymatic activity is not because of protein stability, as our thermodynamic analysis indicates that monomeric mutants require similar energy to unfold and that both point and deletion mutants present similar secondary structure.

Several studies using crystal structures of monomeric TIMs from *T. brucei* conclude that alterations in the geometry of their catalytic residues Lys13 and His95 are responsible for a substantial decrease in catalytic activity [18, 20, 30]. Crystal structures of TvTIM- Δ loop3 deletions shown that their catalytic amino acids Lys13 and His95 are reoriented with respect to their position in wild-type TvTIMs. To understand if the differences in enzymatic activity could be correlated with differences in substrate binding, we measured the dimer-monomer equilibrium exhibited by monomeric TvTIM mutants using different concentrations of the transition state analog PGH (**Fig. 4 and Table 3**). Although all mutants crystallize as dimers, AUC analysis indicate that point mutants, but not loop 3 deletion mutants, assemble as dimers in the presence of PGH. The lack of electron density present in TvTIM1- Δ loop3 is reminiscent of the crystal structure of a TvTIM1-Ile45Tyr ball and socket mutant that lacks electron density for residues Phe66 to Phe73 in loop 3. This ball and socket point mutant decreases the enzymatic activity by near 500-fold [23], a value that is near the 1502-fold reduction observed in TvTIM1- Δ loop3.

The catalytic differences between TvTIM1- Δ loop3 and TvTIM2- Δ loop3 correlates with the increased disorder observed in these crystal structures. In these structures, residues flanking the catalytic His are not observed in the electron density map. It is intriguing how the Ile45Tyr point mutant at residue 45 creates a distorted loop 3 that impedes the monomer to pack against α helices 4 and 5. In the case of loop 3 deletions the shortening of the loop decreases the surface contact between loop 3 and α helices 4 and 5 creating a flexible area that alters the correct packing of loop 3 against the neighbor subunit (**Fig. S2**).

Our results indicate that disrupting loop3 or altering the ball and socket interaction by site directed mutagenesis hampers dimer formation in TvTIMs. However, the fate of the monomeric mutants differs upon substrate addition. In the case of point mutants, substrate

binding induce dimerization, whereas loop3 deletions are unable to dimerize. The involvement of substrate to assist dimer assembly or the presence of a long-lived dimer can explain the high enzymatic activity exhibited by point mutants [31, 32]. However, deletions in loop3 creates monomeric enzymes that cannot reassemble into a catalytically competent dimeric species (**Fig. 7**). The formation of a well-folded monomer is postulated to be necessary for TIM dimerization [33]. Our results indicate that in TvTIMs the active site is formed after the dimer is assembled and that a well-folded monomer must harbor a defined loop 3 that is essential to assemble the active site amino acids in a proper orientation for catalysis. In our model, stable and well-folded monomers dimerize and a rigid interaction of loop3 with the adjacent monomer promotes the assembly of the active site. Our model is reminiscent of the "consecutive folding-association" mechanisms in which oligomerization promotes the formation of catalytically competent TIM species [14].

MATERIAL AND METHODS

MUTANT CONSTRUCTION AND PROTEIN PURIFICATION

TvTIM1- Δ loop3 and TvTIM2- Δ loop3 mutants were constructed using the Quick Change method having the constructs TvTIM1 and TvTIM2 as templates [16, 23]. Wild-type and TvTIMs mutants were purified as previously reported [16]. Proteins were concentrated at 4 mg ml⁻¹ and stored at 4°C for not more than 2 weeks.

DIMER-MONOMER EQUILIBRIUM BY GEL FILTRATION

Gel filtration experiments were conducted in an AKTA-FPLC using a Superdex 75 10/300 GL (GE) at 25 °C. The buffer used was 20 mM Tris pH 7.4, 100 mM NaCl, 1mM DTT or 100 mM triethanolamine pH 7.4, 100 mM NaCl, 1mM DTT. Wild type and mutants were injected at 1 mg ml⁻¹ and in both cases the flow rate was 0.5 ml ml⁻¹. Elution profiles were monitored by absorbance at 280 nm.

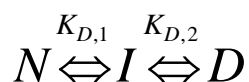
THERMODYNAMIC CHARACTERIZATION

Fluorescence emission scans were obtained using a Perkin Elmer LS-55 Spectrofluorometer at 25 °C and recorded from 320 to 400 nm using an excitation wavelength of 280 nm (2.5 nm bandpass) with a 1 cm path-length cell. Far-UV CD spectra were measured using a JASCO J-815 spectropolarimeter (Jasco Inc., Easton, MD) equipped with a PFD-425S Peltier-type cell holder for temperature control and magnetic stirring. Scans were taken between 200 to 250 nm, at a scan rate of 10 nm min⁻¹ using a 1.0 cm path-length cuvette. Ellipticities are reported as mean residue ellipticity. Chemical denaturation experiments were performed using GdnHCl as denaturant. The methods described in previous work [23] or in the supplementary material.

GDNHCL INDUCED UNFOLDING/REFOLDING DATA ANALYSIS

Chemical denaturation experiments were performed using GdnHCl as denaturant and the methods described in detail for wild-type TvTIMs [22].

The chemical denaturation transitions of the of point mutants and deletions were fit to a three-state denaturation model:



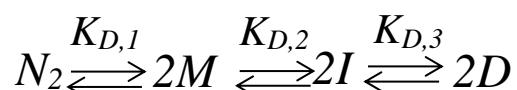
where N , I , and D are native, intermediate, and unfolded protein, respectively. $K_{D,1}$ and $K_{D,2}$ are the equilibrium constants for each folding step, respectively. The fitting equation was

$$y = \frac{y_N + y_I e^{\left[\frac{-\Delta G_{NI}^{H_2O} - m_{NI}[d]}{RT} \right]} + y_D e^{\left[\frac{-\Delta G_{ND}^{H_2O} - m_{ND}[d]}{RT} \right]}}{1 + e^{\left[\frac{-\Delta G_{NI}^{H_2O} - m_{NI}[d]}{RT} \right]} + e^{\left[\frac{-\Delta G_{ND}^{H_2O} - m_{ND}[d]}{RT} \right]}} \quad (8)$$

where d is the concentration of denaturant, $\Delta G_{NI}^{H_2O}$ and $\Delta G_{ND}^{H_2O}$ are the free energy change in the absence of denaturant, and m_{NI} and m_{ND} represent constants of proportionality relating to the solvent exposure difference between native and denatured states and y_N , y_I , and y_D

are the specific signal of native, intermediate, and unfolded protein, respectively, R represent the gas constant and T the absolute temperature.

The Gdn-HCl-induced denaturation transitions of dimeric TvTIM constructs were globally fit over all concentrations of protein to a four-state dimer denaturation model involving two monomeric intermediates according to the scheme



Where the protein is assumed to be in either the native homodimeric state (N_2), two monomeric states depicted as M or I , or in an unfolded monomeric state (D), and $K_{D,1}$, $K_{D,2}$, and $K_{D,3}$ are the equilibrium constants for the three steps, respectively. In this case, the fitting equation has been developed and thoroughly described elsewhere [22].

IN VIVO COMPLEMENTATION ASSAYS

Three independent colonies of *E. coli* BL21 Δ tpi DE3 strain complemented with TvTIM constructs were grown on minimal media agar plates lacking six carbon sugars as previously described [13].

KINETIC CONSTANTS

Kinetic constants were calculated using the method of Plaut and Knowles [34]. Briefly, the forward reaction of triosephosphate isomerase activity was measured at 25 °C using D-glyceraldehyde 3-phosphate (DGAP) as a substrate. NADH oxidation was detected by absorbance changes at 340 nm using an enzyme-coupled reaction with α -glycerophosphate dehydrogenase (GDH). Routinely, 1.0 mL of 100 mM triethanolamine buffer (pH 7.4) contained 10 mM EDTA, 0.20 mM NADH, 1.0 mM DGAP, and 0.01 mg of GDH. DGAP concentrations ranged from 0.05 to 3.0 mM for determination of catalytic

constants. Kinetic parameters were calculated from the initial velocities at each substrate concentration.

ANALYTICAL ULTRACENTRIFUGATION

Protein concentration was determined by absorbance in 280 nm using a spectrophotometer V-530/JASCO. All AUC experiments were performed on an XL-A analytical ultracentrifuge (Beckman, Fullerton, CA) with an An-50 Ti rotor after sample centrifugation at 10,000 rpm for 5 min (4 °C). Sedimentation velocity (SV) experiments were performed in a double-sector epon charcoal-filled centerpiece at 20 °C with a rotor speed of 40,000 rpm. Sample (420 μ L) and reference/buffer (440 μ L) solutions with or without different concentrations of PGH substrate were loaded into the centerpiece. Absorbance at 280 nm was chosen to detect the protein, which was monitored in a continuous mode with a step size of 0.003 cm. It was used protein at 1 mg mL⁻¹ (Absorbance_{280nm} ~1.0) free or with substrate in three different concentrations (47, 187 and 750 μ M). Around 200 scans at different time intervals were acquired and then fitted to a continuous c(s) distribution model using the SEDFIT program. The partial specific volume of protein, the solvent density, and the viscosity were calculated by SEDNTERP.

PROTEIN CRYSTALLIZATION, STRUCTURE DETERMINATION AND REFINEMENT

Δ loop3 deletion mutants and TvTIM2-Val45Ala crystallized in similar conditions that wild-type TvTIMs as previously reported (0.2 M calcium acetate, 0.1 M sodium cacodylate pH 6.5 and 18% PEG 8000) (Estrella, et al., manuscript in preparation). Protein crystals were cryo-protected with mother liquid supplemented with 20% glycerol. Crystals were flash frozen in liquid N₂. Native data were collected at APS and BNL and processed with MolSflm. X-ray structures were solved by molecular replacement using a truncated to poly-Ala model of TvTIM1 with PHENIX-MR [35]. Structure refinement and model rebuilding were carried out with the programs PHENIX and COOT [36] through several cycles of simulated annealing and manual model adjustment to improve the fit to likelihood-weighted electron-density maps. Data collection statistics and refinement are given in **Table 1S**.

SYNTHESIS OF CYCLOHEXYLAMINE SALT OF PHOSPHOGLYCOLOHYDROXAMATE (PGH)

PGH was synthesized from glycolamide based on previous reports [37, 38]. Briefly, the phosphorylation of glycolamide (10 mmol) by polyphosphoric acid (4 mL) was carried out at 45 °C under vacuum on a rotary evaporator for 1 h. pH was adjusted with solid barium carbonate and barium hydroxide until pH 8 was reached. The mixture was filtered and the filtrate was lyophilized. This barium salt (1 mmol) was shaken with water and an excess of Dowex 50WX4-200R (H⁺). The resin was then filtered and 0.7 mL of hydroxylamine solution 50% in H₂O (11.4 mmol) was added. The reaction mixture was kept overnight at room temperature, and lyophilized again. The resulting solid was dissolved in water with 3 mmol of cyclohexylamine. Finally, the solid was re-crystallized from hot ethanol. The purity of the cyclohexylamine salt of PGH was assessed by ¹H, ¹³C, and ³¹P NMR spectra that were recorded using an Agilent 400-VNMRS (for ¹H and ¹³C) and a Varian Inova-300 spectrometers (for ³¹P). The NMR signals are: ¹H NMR (400 MHz, D₂O): δ = 0.99-1.08 (m, 2H, CH₂), 1.13-1.25 (m, 8H, CH₂), 1.48-1.52 (m, 2H, CH₂), 1.64-1.70 (m, 4H, CH₂), 1.80-1.85 (m, 4H, CH₂), 2.96-3.03 (m, 2H, CH), 4.16 (d, $J_{H,P}$ = 6.9 Hz, 2H, CH₂). ¹³C NMR (100 MHz, D₂O): δ = 23.7 (4xCH₂), 24.2 (2xCH₂), 30.3 (4xCH₂), 50.3 (2xCH), 62.4 (d, $J_{C,P}$ = 5.03 Hz, CH₂), 169.7 (d, $J_{C,P}$ = 8.05 Hz, C=O). ³¹P NMR (121.5 MHz, D₂O): δ = 3.40 (s, 1P). The concentration of the solution of PGH was determined by a colorimetric assay of the inorganic phosphate released by alkaline phosphatase [39].

ACKNOWLEDGEMENTS

We thank Professor Thomas J. Magliery (Ohio State University) for *E. coli* Δ TIM *DE3* strain. This work was supported by CONACYT-Fronteras de la Ciencia Grant # 11 to LGB. We thank the staff of NSLS beamline X6A for data-collection facilities.

Author contributions:

PJS, JLVS, MLH, GVJ, CDQ, LFAN, GMM, JF, AJDS, performed experiments. ERP, RSS, SLG; PJS, Solved crystal structures, ACMF, CGBC, analyzed data, LGB Conceived the project and analyzed data. CGBC, PJS, and LGB; wrote the manuscript

Fig. 1 Dimer-monomer equilibrium of TvTIM mutants monitored by gel-filtration **A)** Structural context of loop3 and ball and socket interactions in TvTIM1 and TvTIM2. Each TvTIM1 monomer is colored in orange and grey. Residue Ile45 and loop 3 of each subunit are colored as their corresponding monomer. **B)** Elution profile of TvTIM1 point and deletion mutants in comparison to TvTIM1 (black trace). TvTIM1-Ile45Ala (red trace) and TvTIM1- Δ loop 3 (blue trace) elute in a volume that corresponds to a protein of 23 kDa, whereas the elution profile of TvTIM corresponds to a protein of 46 kDa **C)** Elution profile of TvTIM2 point and deletion mutants in comparison to wild-type TvTIM1. The elution profiles of TvTIM2-Val45Ala (magenta trace) and TvTIM2- Δ loop3 (orange trace) are compared to the elution profile of dimeric TvTIM1 (black trace). **D)** SDS-PAGE showing the purified TvTIMs proteins before their injection into the S-75 Column. Lane 1, TvTIM1; lane 2, TvTIM1- Δ loop 3; lane 3, TvTIM1-Ile45Ala; lane 4, TvTIM2- Δ loop 3; lane 5, TvTIM2-Val45Ala.

Fig. 2 *In vivo* complementation assays of TvTIM1 and TvTIM2 mutants. **A)** *E. coli* Δ *tpi* Keio (*DE3*) strain transformed with plasmids expressing point and deletion mutants. After an incubation of 48 hours, point mutants TvTIM1-Ile45Ala and TvTIM2-Val45Ala are able to complement, whereas loop 3 deletions are unable to complement the *E. coli* Δ *tpi* strain. **B)** *In vivo* complementation in minimal liquid medium. Growth curves of cells were obtained at 37 °C for 48 hours by measuring the optical density at 600 nm.

Fig. 3 Denaturation and unfolding profiles of point and deletion mutants. Gdn-HCl denaturation profiles of point and deletion mutants monitored by intrinsic fluorescence spectroscopy (panels A and B). Protein samples were present at 30 μ g mL⁻¹ in 20 mM Tris-HCl pH 7.4. Unfolding profiles of point and deletion mutants monitored by ANS fluorescence (panels C and D).

Fig 4 Sedimentation coefficient distributions for TvTIM1 and its monomeric mutants in the absence and in the presence of 0.75 mM PGH. The traces for TvTIM1, TvTIM1- Δ loop 3, TvTIM1-Ile45Ala; TvTIM2- Δ loop 3; and TvTIM2-Val45Ala are indicated in the inset. The equilibrium of pointTvTIM1 and TvTIM2 monomeric mutants is displaced towards the dimeric state in presence of PGH. For instance, TvTIM1-Ile45Ala is populated in a 9% of dimer in solution in the absence of PGH and this mutant reaches a 68% of dimeric population

at 0.75 mM of PGH. The same behavior is observed for TIM2-Val45Ala which is presented as 17% dimer in solution in the absence of PGH. The amount of dimer TIM2-Val45Ala increases to 73% with 0.75 mM PGH. The mutants that have a deletion in loop3, remain mostly as monomer in solution upon the addition of 1 mM PGH. TIM1- Δ loop3 and TIM2- Δ loop3 present near 98% of the population in monomer form in solution in the absence of PGH and 91% with 0.75 PGH. TvTIM1 was used as a control for the experiment. This protein is a dimer in solution even in the absence of the substrate analog PGH.

Fig. 5 Ribbon representation of wild-type TvTIMs and mutants showing their B-factors. Ribbon representation of dimeric TvTIMs showing the B-factor. Normalized scale bar is colored from blue to red. The location of loop3 and loop 4 with increased thermal motion in TvTIM- Δ loop 3 mutants is indicated by an arrow.

Fig 6 Structural changes between wild-type TvTIM2 and TvTIM2 Δ loop3. A) C α superposition between wild-type TvTIM2 and TvTIM2- Δ loop 3 mutant. The catalytic amino acids are presented in a ball-stick representation. A 30 and 60 ° rotation shows the movement in the α helix 4 of the TvTIM2- Δ loop 3 mutant that alters the position of the catalytic histidine.

Fig 7 Proposed model explaining the loss of activity observed monomeric Δ loop3 mutants in contrast to the high enzymatic activity present in monomeric point mutants. Both point and deletion mutants originated stable monomeric species. The loss of loop3 originates a repacking in the dimer interface that alters the conformation of catalytic amino acids. The lost of a competent active site hampers reassembly in response to substrate concentration in Δ loop3 mutants.

Table 1 Kinetic characterization of TvTIM mutants

Table 2 Thermodynamic parameters for wild type and mutants

Table 3 Dimerization of monomeric TvTIMs in the presence of PGH.

ACCEPTED MANUSCRIPT

REFERENCES

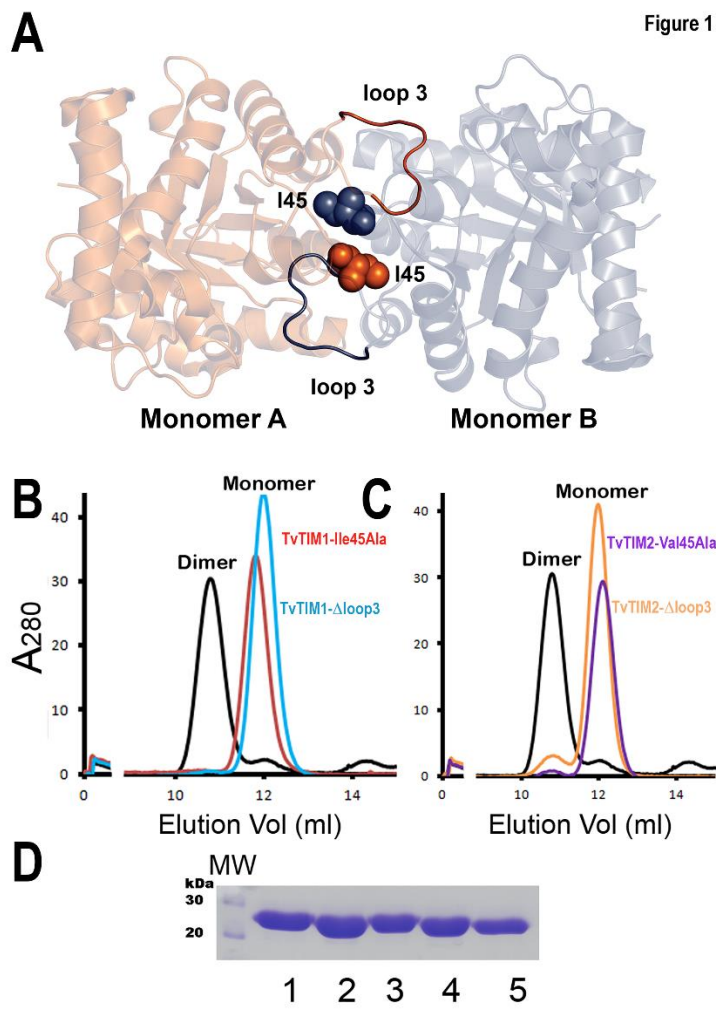
- [1] M. Lynch, The evolution of multimeric protein assemblages, *Mol Biol Evol*, 29 (2012) 1353-1366.
- [2] N.J. Marianayagam, M. Sunde, J.M. Matthews, The power of two: protein dimerization in biology, *Trends Biochem Sci*, 29 (2004) 618-625.
- [3] J.P. Richard, X. Zhai, M.M. Malabanan, Reflections on the catalytic power of a TIM-barrel, *Bioorg Chem*, 57 (2014) 206-212.
- [4] R.K. Wierenga, E.G. Kapetaniou, R. Venkatesan, Triosephosphate isomerase: a highly evolved biocatalyst, *Cell Mol Life Sci*, 67 (2010) 3961-3982.
- [5] M. Kohlhoff, A. Dahm, R. Hensel, Tetrameric triosephosphate isomerase from hyperthermophilic Archaea, *FEBS Lett*, 383 (1996) 245-250.
- [6] H. Walden, G.S. Bell, R.J. Russell, B. Siebers, R. Hensel, G.L. Taylor, Tiny TIM: a small, tetrameric, hyperthermostable triosephosphate isomerase, *J Mol Biol*, 306 (2001) 745-757.
- [7] M. Banerjee, H. Balaram, P. Balaram, Structural effects of a dimer interface mutation on catalytic activity of triosephosphate isomerase. The role of conserved residues and complementary mutations, *FEBS J*, 276 (2009) 4169-4183.
- [8] K. Maithal, G. Ravindra, G. Nagaraj, S.K. Singh, H. Balaram, P. Balaram, Subunit interface mutation disrupting an aromatic cluster in *Plasmodium falciparum* triosephosphate isomerase: effect on dimer stability, *Protein Eng*, 15 (2002) 575-584.
- [9] M. Banerjee, H. Balaram, N.V. Joshi, P. Balaram, Engineered dimer interface mutants of triosephosphate isomerase: the role of inter-subunit interactions in enzyme function and stability, *Protein Eng Des Sel*, 24 (2011) 463-472.
- [10] M. Peimbert, L. Dominguez-Ramirez, D.A. Fernandez-Velasco, Hydrophobic repacking of the dimer interface of triosephosphate isomerase by in silico design and directed evolution, *Biochemistry*, 47 (2008) 5556-5564.

- [11] T.C. Alber, R.C. Davenport, Jr., D.A. Giammona, E. Lolis, G.A. Petsko, D. Ringe, Crystallography and site-directed mutagenesis of yeast triosephosphate isomerase: what can we learn about catalysis from a "simple" enzyme?, *Cold Spring Harb Symp Quant Biol*, 52 (1987) 603-613.
- [12] D.W. Banner, A.C. Bloomer, G.A. Petsko, D.C. Phillips, C.I. Pogson, I.A. Wilson, P.H. Corran, A.J. Furth, J.D. Milman, R.E. Offord, J.D. Priddle, S.G. Waley, Structure of chicken muscle triose phosphate isomerase determined crystallographically at 2.5 angstrom resolution using amino acid sequence data, *Nature*, 255 (1975) 609-614.
- [13] B.J. Sullivan, V. Durani, T.J. Magliery, Triosephosphate isomerase by consensus design: dramatic differences in physical properties and activity of related variants, *J Mol Biol*, 413 (2011) 195-208.
- [14] W. Schliebs, N. Thanki, R. Jaenicke, R.K. Wierenga, A double mutation at the tip of the dimer interface loop of triosephosphate isomerase generates active monomers with reduced stability, *Biochemistry*, 36 (1997) 9655-9662.
- [15] E. Lolis, T. Alber, R.C. Davenport, D. Rose, F.C. Hartman, G.A. Petsko, Structure of yeast triosephosphate isomerase at 1.9-Å resolution, *Biochemistry*, 29 (1990) 6609-6618.
- [16] S. Lara-Gonzalez, P. Estrella-Hernandez, A. Ochoa-Leyva, M. Del Carmen Portillo-Tellez, L.A. Caro-Gomez, E.E. Figueroa-Angulo, H. Salgado-Lugo, J.F. Miranda Ozuna, J. Ortega-Lopez, R. Arroyo, L.G. Briebe, C.G. Benitez-Cardoza, Structural and thermodynamic folding characterization of triosephosphate isomerases from *Trichomonas vaginalis* reveals the role of destabilizing mutations following gene duplication, *Proteins*, 82 (2014) 22-33.
- [17] G. Saab-Rincon, V.R. Juarez, J. Osuna, F. Sanchez, X. Soberon, Different strategies to recover the activity of monomeric triosephosphate isomerase by directed evolution, *Protein Eng*, 14 (2001) 149-155.

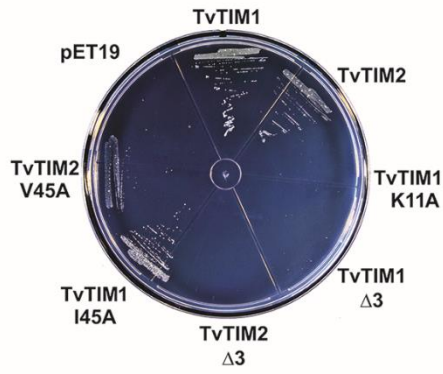
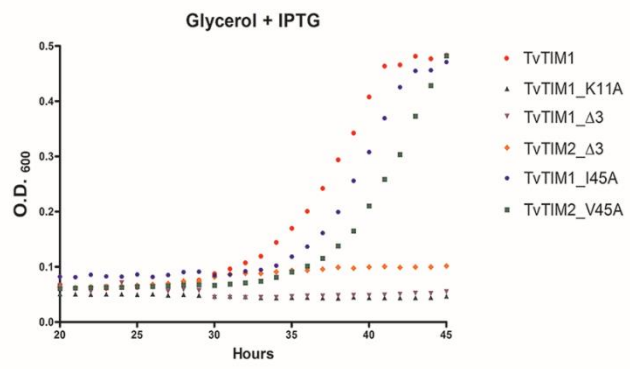
- [18] T.V. Borchert, R. Abagyan, R. Jaenicke, R.K. Wierenga, Design, creation, and characterization of a stable, monomeric triosephosphate isomerase, *Proc Natl Acad Sci U S A*, 91 (1994) 1515-1518.
- [19] F. Zarate-Perez, M.E. Chanez-Cardenas, R. Arreola, A. Torres-Larios, E. Vazquez-Contreras, Different catalytic properties of two highly homologous triosephosphate isomerase monomers, *Biochem Biophys Res Commun*, 382 (2009) 626-630.
- [20] T.V. Borchert, K.V. Kishan, J.P. Zeelen, W. Schliebs, N. Thanki, R. Abagyan, R. Jaenicke, R.K. Wierenga, Three new crystal structures of point mutation variants of monoTIM: conformational flexibility of loop-1, loop-4 and loop-8, *Structure*, 3 (1995) 669-679.
- [21] J.F. Miranda-Ozuna, M.S. Hernandez-Garcia, L.G. Briebe, C.G. Benitez-Cardoza, J. Ortega-Lopez, A. Gonzalez-Robles, R. Arroyo, The Glycolytic Enzyme Triosephosphate Isomerase of *Trichomonas vaginalis* Is a Surface-Associated Protein Induced by Glucose That Functions as a Laminin- and Fibronectin-Binding Protein, *Infect Immun*, 84 (2016) 2878-2894.
- [22] E.E. Figueroa-Angulo, P. Estrella-Hernandez, H. Salgado-Lugo, A. Ochoa-Leyva, A. Gomez Puyou, S.S. Campos, G. Montero-Moran, J. Ortega-Lopez, G. Saab-Rincon, R. Arroyo, C.G. Benitez-Cardoza, L.G. Briebe, Cellular and biochemical characterization of two closely related triosephosphate isomerases from *Trichomonas vaginalis*, *Parasitology*, 139 (2012) 1729-1738.
- [23] S. Lara-Gonzalez, P. Estrella, C. Portillo, M.E. Cruces, P. Jimenez-Sandoval, J. Fattori, A.C. Migliorini-Figueira, M. Lopez-Hidalgo, C. Diaz-Quezada, M. Lopez-Castillo, C.H. Trasvina-Arenas, E. Sanchez-Sandoval, A. Gomez-Puyou, J. Ortega-Lopez, R. Arroyo, C.G. Benitez-Cardoza, L.G. Briebe, Substrate-Induced Dimerization of Engineered Monomeric Variants of Triosephosphate Isomerase from *Trichomonas vaginalis*, *PLoS One*, 10 (2015) e0141747.
- [24] H. Najera, M. Costas, D.A. Fernandez-Velasco, Thermodynamic characterization of yeast triosephosphate isomerase refolding: insights into the interplay between function and stability as reasons for the oligomeric nature of the enzyme, *Biochem J*, 370 (2003) 785-792.

- [25] R.K. Wierenga, M.E. Noble, G. Vriend, S. Nauche, W.G. Hol, Refined 1.83 Å structure of trypanosomal triosephosphate isomerase crystallized in the presence of 2.4 M-ammonium sulphate. A comparison with the structure of the trypanosomal triosephosphate isomerase-glycerol-3-phosphate complex, *J Mol Biol*, 220 (1991) 995-1015.
- [26] S.C. Mande, V. Mainfroid, K.H. Kalk, K. Goraj, J.A. Martial, W.G. Hol, Crystal structure of recombinant human triosephosphate isomerase at 2.8 Å resolution. Triosephosphate isomerase-related human genetic disorders and comparison with the trypanosomal enzyme, *Protein Sci*, 3 (1994) 810-821.
- [27] D. Straus, R. Raines, E. Kawashima, J.R. Knowles, W. Gilbert, Active site of triosephosphate isomerase: in vitro mutagenesis and characterization of an altered enzyme, *Proc Natl Acad Sci U S A*, 82 (1985) 2272-2276.
- [28] S.C. Blacklow, R.T. Raines, W.A. Lim, P.D. Zamore, J.R. Knowles, Triosephosphate isomerase catalysis is diffusion controlled. Appendix: Analysis of triose phosphate equilibria in aqueous solution by ^{31}P NMR, *Biochemistry*, 27 (1988) 1158-1167.
- [29] W. Schliebs, N. Thanki, R. Eritja, R. Wierenga, Active site properties of monomeric triosephosphate isomerase (monoTIM) as deduced from mutational and structural studies, *Protein Sci*, 5 (1996) 229-239.
- [30] M.M. Malabanan, M.K. Go, T.L. Amyes, J.P. Richard, Wildtype and engineered monomeric triosephosphate isomerase from *Trypanosoma brucei*: partitioning of reaction intermediates in D₂O and activation by phosphite dianion, *Biochemistry*, 50 (2011) 5767-5779.
- [31] M.G. Botelho, A.W. Rietveld, S.T. Ferreira, Long-lived conformational isomerism of protein dimers: the role of the free energy of subunit association, *Biophys J*, 91 (2006) 2826-2832.
- [32] V.H. Moreau, A.W. Rietveld, S.T. Ferreira, Persistent conformational heterogeneity of triosephosphate isomerase: separation and characterization of conformational isomers in solution, *Biochemistry*, 42 (2003) 14831-14837.

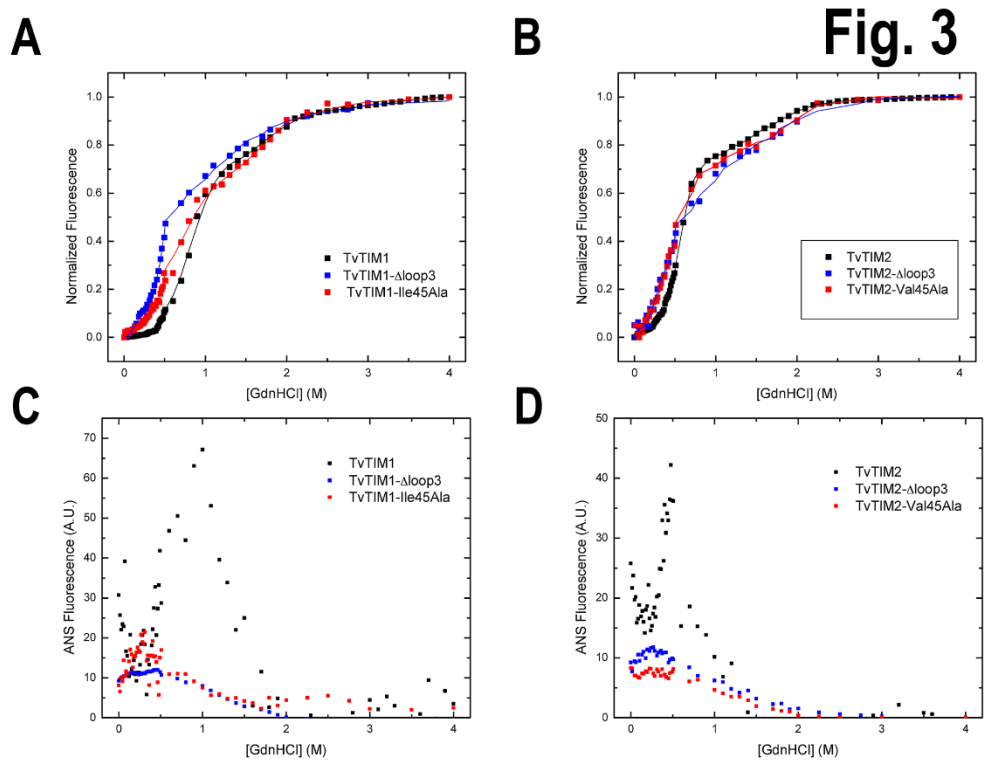
- [33] C.J. Morgan, D.K. Wilkins, L.J. Smith, Y. Kawata, C.M. Dobson, A compact monomeric intermediate identified by NMR in the denaturation of dimeric triose phosphate isomerase, *J Mol Biol*, 300 (2000) 11-16.
- [34] B. Plaut, J.R. Knowles, pH-dependence of the triose phosphate isomerase reaction, *Biochem J*, 129 (1972) 311-320.
- [35] P.D. Adams, P.V. Afonine, G. Bunkóczy, V.B. Chen, I.W. Davis, N. Echols, J.J. Headd, L.-W. Hung, G.J. Kapral, R.W. Grosse-Kunstleve, PHENIX: a comprehensive Python-based system for macromolecular structure solution, *Acta Crystallographica Section D: Biological Crystallography*, 66 (2010) 213-221.
- [36] P. Emsley, B. Lohkamp, W.G. Scott, K. Cowtan, Features and development of Coot, *Acta Crystallographica Section D: Biological Crystallography*, 66 (2010) 486-501.
- [37] P. Weber, M. Fonvielle, M. Therisod, New facile synthesis of phosphoglycolohydroxamic acid and other phosphoglycolic acid derivatives, *Tetrahedron Lett.*, 44 (2003) 9047-9049.
- [38] S.D. Pegan, K. Rukseree, G.C. Capodagli, E.A. Baker, O. Krasnykh, S.G. Franzblau, A.D. Mesecar, Active site loop dynamics of a class IIa fructose 1,6-bisphosphate aldolase from *Mycobacterium tuberculosis*, *Biochemistry*, 52 (2013) 912-925.
- [39] B. Ames, Assay of inorganic phosphate, total phosphate and phosphatases, *Methods Enzymol*, 8 (1966) 115-118.

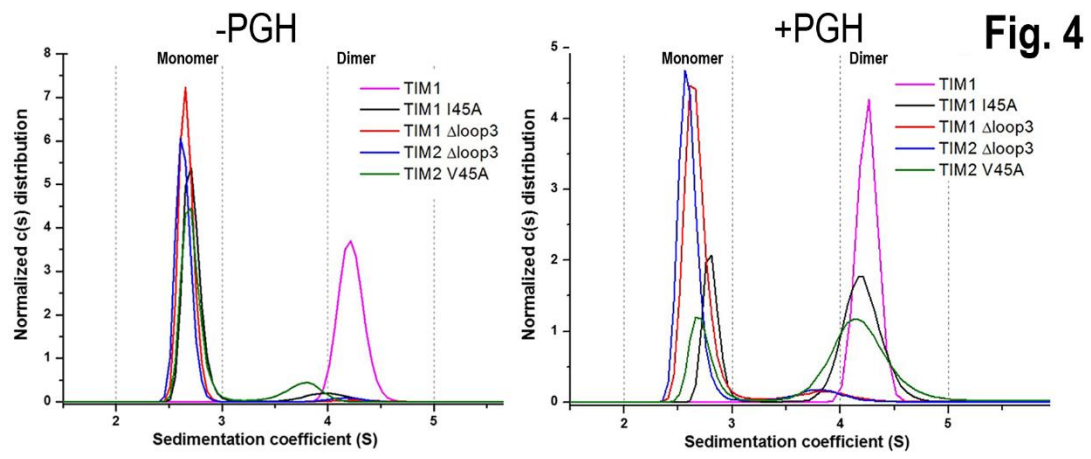


ACCEPTED

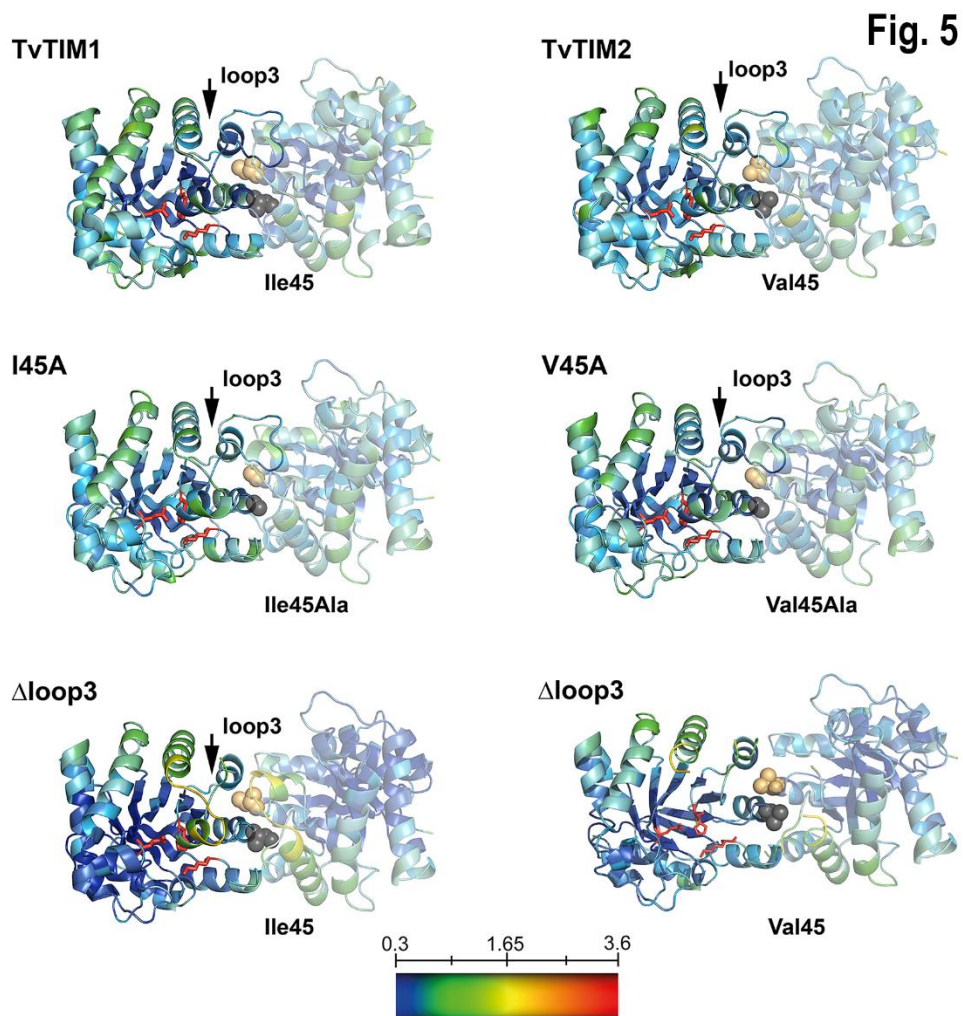
A**B****Fig. 2**

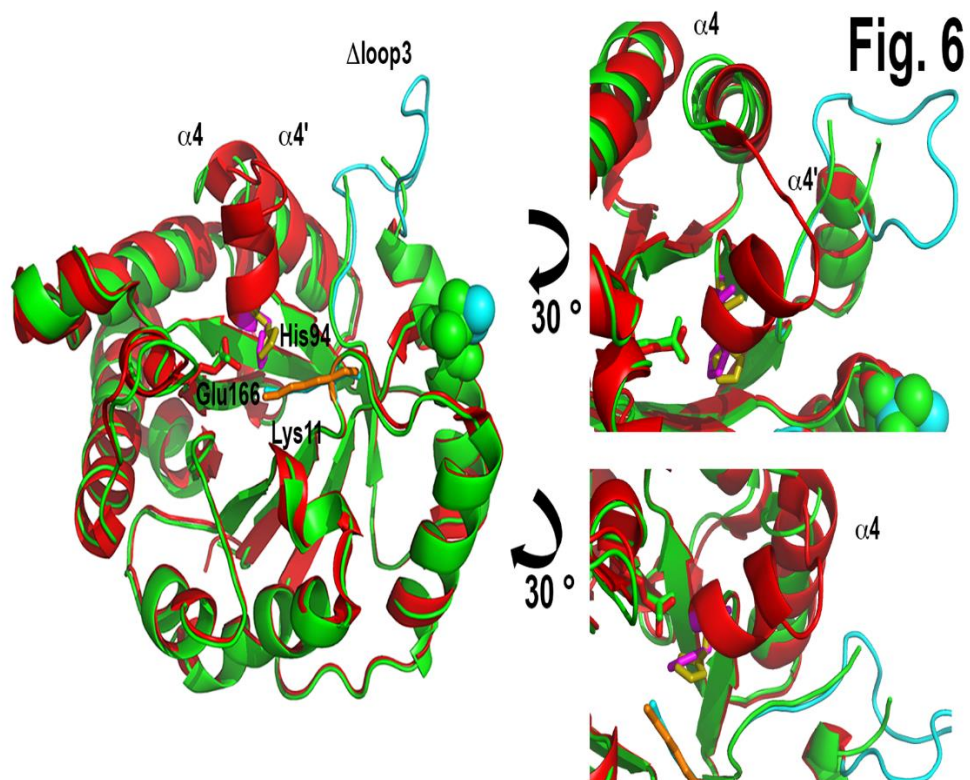
ACCEPTED MANUSCRIPT



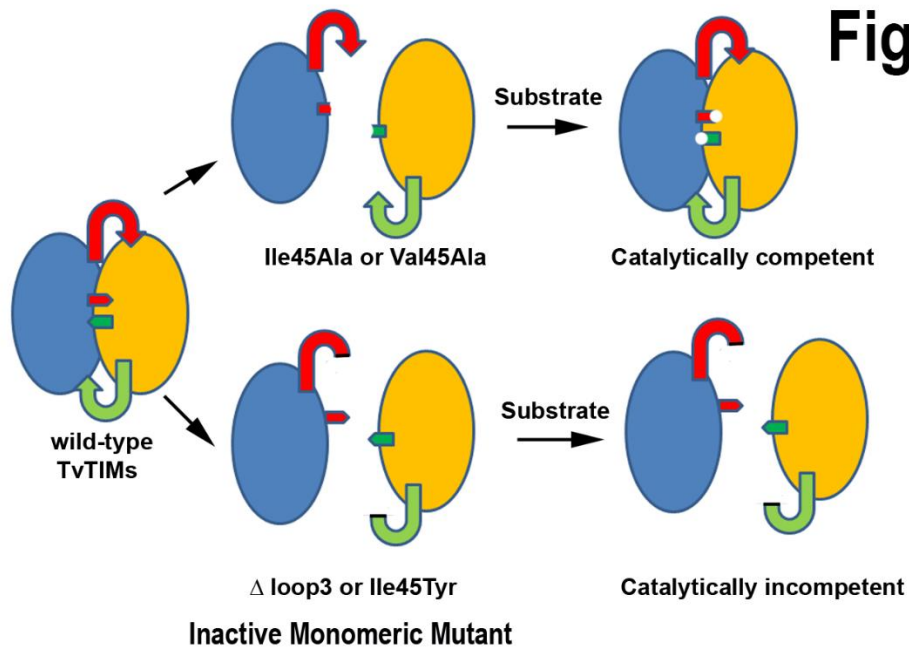


ACCEPTED MANUSCRIPT





ACCEPTED MA



ACCEPTED MANUSCRIPT

Table 1 Catalytic parameters of ball and socket and Δ loop3 TvTIMs mutants

Enzyme	K_M (mM)	K_{cat} (min^{-1})	K_{cat}/K_M ($\text{mM}^{-1} \text{min}^{-1}$)	fold decrease in catalytic efficiency	Reference
TvTIM1	0.23 ± 0.019	7.98×10^4	3.5×10^5	1	(Figuroa-Angulo et al., 2012)
Ile45Ala	0.392 ± 0.036	4.7×10^3	1.19×10^4	29	Lara-Gonzalez, 2015
TIM1 Δ loop3	0.402 ± 0.029	9.4×10^1	2.33×10^2	1502	This work
TvTIM2	0.21 ± 0.024	8.24×10^4	3.8×10^5	1	(Figuroa-Angulo et al., 2012)
Val45Ala	0.514 ± 0.020	4.6×10^3	8.95×10^3	39	This work
TIM2 Δ loop3	0.503 ± 0.031	1.9×10^1	3.7×10^1	9400	This work

ACCEPTED MANUSCRIPT

Table 2 Thermodynamic Parameters for TvTIM1 and TvTIM2^c.

Dimeric Constructs Model: N ₂ ↔2M↔2I↔2D				
Construct	$\Delta G_{N_2 2M}^{H_2O}$ kJ mol ⁻¹	$\Delta G_{MI}^{H_2O}$ kJ mol ⁻¹	$\Delta G_{ID}^{H_2O}$ kJ mol ⁻¹	^a $\Delta G_{D,tot}^{H_2O}$ kJ mol ⁻¹
TvTIM1	48.8 (±3.0)	84.0 (±5.5)	23.3 (±2.0)	263.4 (±18.0)
TvTIM2	15.5 (±2.5)	53.8 (±3.0)	6.7 (±0.8)	136.5 (±10.1)

$${}^a \Delta G_{D,tot}^{H_2O} = \Delta G_{N_2 2M}^{H_2O} + 2 \Delta G_{MI}^{H_2O} + 2 \Delta G_{ID}^{H_2O}$$

Monomeric Constructs Model: N↔I↔D			
Construct	$\Delta G_{Ni}^{H_2O}$ kJ mol ⁻¹	$\Delta G_{ID}^{H_2O}$ kJ mol ⁻¹	^b $\Delta G_{D,tot}^{H_2O}$ kJ mol ⁻¹
TvTIM1-Ile45Ala	27.1 (±3.0)	39.2 (±1.1)	66.3 (±4.1)
TvTIM1- Δ loop3	15.3 (±1.8)	28.2 (±1.5)	43.5 (±3.3)
TvTIM2-Val45Ala	16.7(±1.7)	30.2 (±1.5)	46.9 (±3.2)
TvTIM2- Δ loop3	12.4 (±1.5)	27.6 (±1.5)	40 (±3.0)

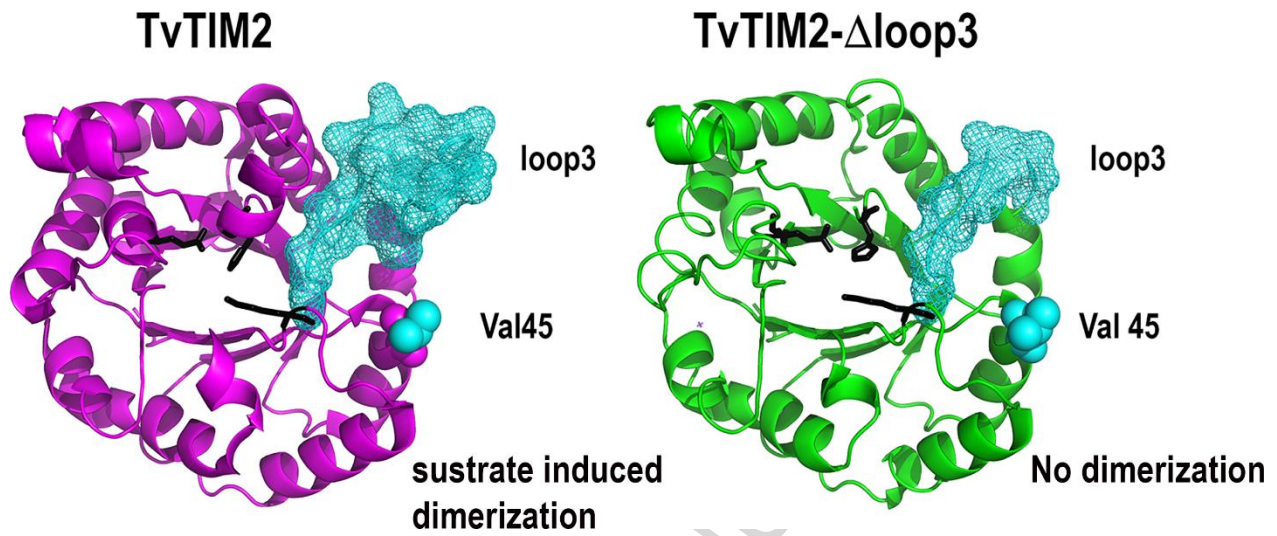
$${}^b \Delta G_{D,tot}^{H_2O} = \Delta G_{Ni}^{H_2O} + \Delta G_{ID}^{H_2O}$$

^c Global analysis was performed with the non-linear, least-squares fitting program Origin , version 8. Errors quoted are the standard errors calculated by the fitting program.

Table 3 PGH alters the dimer monomer equilibrium in monomeric TvTIMs

Protein	NO PGH		+ 47 μ M PGH		+ 187 μ M PGH		+ 750 μ M PGH	
	%MON	%DIM	%MON	%DIM	%MON	%DIM	%MON	%DIM
TIM1 - Control	-	99.95 \pm 0.05	-	99.5 \pm 0.5	-	99.7 \pm 0.2	-	99.7 \pm 0.1
TIM1 I45A	91 \pm 1	8 \pm 1	56 \pm 2	43 \pm 1	38 \pm 2	61 \pm 2	31 \pm 2	68 \pm 2
TIM1 Δ loop3	97 \pm 1	2 \pm 1	95 \pm 1	4 \pm 1	94.9 \pm 0.9	4.6 \pm 0.5	91 \pm 1	8 \pm 1
TIM2 Δ loop3	95 \pm 1	3.5 \pm 0.4	91 \pm 1	7 \pm 1	97 \pm 1	2.6 \pm 0.3	90 \pm 1	9 \pm 1
TIM2 V45A	82 \pm 1	17 \pm 1	61 \pm 2	37 \pm 2	35 \pm 2	64 \pm 2	26 \pm 2	72 \pm 1

Graphical Abstract



ACCEPTED MANUSCRIPT

Highlights

- Dimer assembly in Triosephosphate isomerase requires a competent active site
- Crystal structures of monomeric triosephosphate isomerases
- Substrate induced dimerization

ACCEPTED MANUSCRIPT